Journal of Alloys and Compounds 1009 (2024) 176755

Contents lists available at ScienceDirect

Journal of Alloys and Compounds

journal homepage: www.elsevier.com/locate/jalcom

A structural, magnetic and colloidal stability study of uncoated and silica coated iron oxide samples prepared in two different surfactants

E. Hernán [a,*], J. Isasi [a,*], M. Rapp [a], M. Alcolea Palafox [b], J.F. Marco [c]

[a] Departamento de Química Inorgánica, Facultad de Ciencias Químicas, Universidad Complutense de Madrid, Ciudad Universitaria s/n, Madrid 28040, Spain
[b] Departamento de Química Física, Facultad de Ciencias Químicas, Universidad Complutense de Madrid, Ciudad Universitaria s/n, Madrid 28040, Spain
[c] Instituto de Química Física Blas Cabrera, Consejo Superior de Investigaciones Científicas, Serrano 119, Madrid 28006, Spain

ARTICLE INFO

Keywords:
Iron oxide samples. Mössbauer spectroscopy. Magnetic behaviour. Colloidal stability

ABSTRACT

The discovery of new magnetic materials of interest in the biomedicine field is a relevant topic in current research. For years, our research group has been investigating the obtaining and study of nanostructured magnetic samples that behave superparamagnetically to enable their transport in living organisms. We present here a study that summarizes the structural characteristics, magnetic behavior and stability of two Fe_3O_4 samples synthesized by coprecipitation that were dispersed using two different surfactants (oleylamine, OL, and oleic acid, OA), and two others prepared from the previous ones by reaction with tetraethyl orthosilicate (TEOS). The relationships between the surfactant used in the synthesis, the presence of a certain maghemite (γ-Fe_2O_3) content, the influence of silica shell thickness and magnetic behaviour of all samples were systematically studied by X-ray diffraction (XRD), Fourier transform infrared spectroscopy (FTIR), transmission electron microscopy (TEM), Mössbauer spectroscopy and H *vs.* M loops. Rietveld refinements of the XRD profiles confirmed a partial oxidation of the non-silica-coated samples and FTIR spectra of the uncoated samples showed a very strong broad metal-oxygen band and additional sets of bands from the different organic chains of the two surfactants. Individual particles with a mean diameter of 7 and 9 nm were distinguished in TEM images of uncoated magnetic samples. Mössbauer data indicated the presence of non-stoichiometric magnetite in all samples, in agreement with XRD refinements. Magnetic measurements confirmed the superparamagnetic behavior of all the samples. Highest negative zeta potential values are found for the silica covered samples in both acidic and basic medium, being Fe_3O_4-AO@SiO_2 the best suited for the purposes of its dispersibility in future applications. Low polydispersity index (PDI) values confirmed the best stability and dispersibility of all samples investigated in tetrahydrofuran (THF).

1. Introduction

Over the years, the study of nanostructured magnetic samples has aroused great interest due to their remarkable structural characteristics and unique properties that have led to their use in various fields such as chemistry, physics, biology, materials science and engineering [1,2]. Compared to their bulk counterparts, the nanostructured samples contain particles of distinct and small sizes ranging from 1 to 100 nm with a high surface-to-volume ratio. The set of all these parameters determines its mechanical, thermal, electrical, magnetic, and optical properties or its response capacity to magnetic fields [3–7].

Ferrites are important magnetic materials due to their chemical and thermal stability and their unique properties [5–10]. The chemical composition of Fe_3O_4 is described as $(Fe^{3+})_A[(Fe^{3+}Fe^{2+}]_BO_4$ where A and B corresponds to iron ions located in the tetrahedral and octahedral sites, respectively [11,12], of the spinel-related structure. In samples of Fe_3O_4 oxide, Fe^{2+} ions are easily oxidized to Fe^{3+} ions, affecting only the fraction of these ions in the octahedral positions. The resulting oxidized phase, maghemite (γ-Fe_3O_4), predominates when these samples contain small particles, below 10 nanometers, while has been found that the fraction of the magnetite phase gradually increases when the particle size increases [13]. Compared to the magnetite variety, in maghemite iron oxide there are of Fe^{2+} ion vacancies in octahedral sites, so the chemical composition of the oxide is $(Fe_8^{3+})[Fe_{40/3}^{3+}Vacant_{8/3}]O_{32}$, formula that takes into account charge neutrality [14].

Iron oxide nanoparticles in both the magnetite or maghemite phases

* Corresponding authors.
E-mail addresses: esthhe01@ucm.es (E. Hernán), isasi@ucm.es (J. Isasi).

https://doi.org/10.1016/j.jallcom.2024.176755
Received 1 July 2024; Received in revised form 3 September 2024; Accepted 26 September 2024
Available online 2 October 2024

exhibit a practically superparamagnetic behavior and high saturation magnetization depending on their grain size, temperature and stability. The saturation magnetization is higher for magnetite than for maghemite [15]. These unique magnetic characteristics lead to its action being investigated in magnetic recording systems, in biomedicine or even in environmental chemistry for removing toxic cations from non-potable waters [12,16,17]. However, since saturation magnetization values are reduced in magnetic nanoparticles and since many of these applications require samples that have the highest possible saturation magnetization, it is very important to avoid oxidation of these samples as much as possible.

Over the years, numerous preparation methods have been employed for the synthesis of superparamagnetic iron oxide nanoparticles. These methods include thermal decomposition, sol-gel, microemulsion, and coprecipitation among others [18–20]. Once these magnetic samples are obtained, their nanoparticles have hydrophobic surfaces with large area to volume ratio and a tendency to aggregate, resulting in a larger relative particle size [21].

To prevent agglomeration and oxidation by atmospheric oxygen of Fe_3O_4 to γ-Fe_2O_3, protective agents such as polymers or surfactants are usually added during preparation. In our research group we have worked on the coating process of the surface of iron oxide particles with oleic acid and vegetable oils of different degrees of acidity, sodium citrates, polyethylene glycol (PEG), polyvinylpyrrolidone (PVP), chitosan with glutaraldehyde or glyoxal, among other agents [15,22]. Despite everything, in many cases the use of different synthesis methods of Fe_3O_4 samples has led to mixtures of the magnetite and maghemite phases [15,22].

Evaluating the magnetite and maghemite content in iron oxide samples is interesting when trying to analyze the usefulness of magnetic nanoparticles in biomedicine. Mössbauer spectroscopy is a very useful tool for the identification of iron oxide species present in samples of this type [13,15]. The Mössbauer spectra are very sensitive to superparamagnetic effects and their shape can be affected by differences in the particle size distributions or the occurrence or absence of interparticle interactions. This, together with its ability in distinguishing different iron oxidation states present in its composition, as well as its specificity in identifying different iron compounds make this technique a fundamental tool for investigating iron oxide nanoparticle systems.

In the field of biomedicine, it is also essential to evaluate the stability of particles in an aqueous medium. When charged particles are present in solution they are surrounded by species of opposite charge sign. It constitutes the so-called electrical double layer at the particle/solution interface that governs the stability of charged particles in solution. This diffuse shell of ions that is in contact with the bulk medium has an electric charge called zeta (ξ) potential and its value is related to the net charge of the particle surface and the distribution of the electric charge can be calculated by applying an electric field to the constituent particles of the investigated samples and measuring the speed of these particles on their way to the electrodes [23]. After its dispersion in certain solvents, the charge present on its surface can be determined, thus being able to verify its functionalization and better predict its behavior in biomedicine.

Considering all the above, in the present work we describe a complete and comparative study of magnetic samples prepared by coprecipitation with two different surfactants without and with silica addition. For the first time, in this study the relationships between the surfactant used in the synthesis, the presence of a certain maghemite content in the iron oxide samples obtained, the influence of the silica shell thickness, the magnetic behavior and colloidal stability in two different solvents are described.

2. Experimental

2.1. Synthesis of Fe_3O_4 samples

Two magnetic samples were synthesized by coprecipitation method using ferric chloride hexahydrate ($FeCl_3{\cdot}6\ H_2O$, 97 % Strem Chemicals) and ferrous chloride tetrahydrate ($FeCl_2{\cdot}4\ H_2O$, 99 % Sigma-Aldrich) as precursor materials and by considering the reaction (1).

$$2FeCl_3{\cdot}6H_2O + FeCl_2{\cdot}4H_2O + 8NaOH \rightarrow Fe_3O_4 + 8NaCl + 20H_2O \quad (1)$$

The corresponding stoichiometric amounts were deposited in beakers to which 150 mL of deionized water was added (see preparation procedure in Fig. 1.a). The two resulting mixtures were transferred to two-neck glass flasks that were immersed in a thermostatic bath at 75ºC and were subjected to mechanical stirring (200 rpm) under an Ar atmosphere to prevent oxidation of the Fe^{2+} ions. At the same time, a solution of pH ~ 12 was prepared by mixing a stoichiometric amount of NaOH (98–100 % PanReac), 10 mL of deionized water and 3 mL of NH_3 (32 %). This solution was added to the two three necked glass flasks, observing a color change of the chloride solution from orange to black due to the precipitation of the ferric and ferrous hydroxides that took place, as indicated by the reaction (2) [24].

$$Fe^{2+} + 2Fe^{3+} + 8OH^- \rightarrow Fe(OH)_2 + 2Fe(OH)_3 \rightarrow Fe_3O_4 + 4\ H_2O \quad (2)$$

Next, 2 mL of oleic acid (OA, 90 %, Aldrich) was slowly added to one of the threenecked glass flasks, while 2 mL of oleylamine was added to the other. (OL, 70 %, Aldrich). These reactions were maintained for 30 minutes. Both surfactants, oleic acid and oleylamine generate a dispersive medium that facilitates particle size control and prevents agglomeration [25]. These surfactants have different functional groups. Oleic acid is a monounsaturated fatty acid with the expanded chemical formula $CH_3(CH_2)_7CH{=}CH(CH_2)_7COOH$, while oleylamine is an unsaturated fatty amine with an expanded molecular formula $CH_3(CH_2)_7CH{=}CH(CH_2)_7CH_2NH_2$. It is expected that the different functional groups may influence the particle size of the resulting samples. The precipitates obtained were separated by magnetic decantation and washed with acetone to eliminate 2 mL of possible traces of both ammonia and surfactant agent. The resulting black powders were dried at 70 °C for 5 hours. In this work, the black powder samples obtained have been named as Fe_3O_4-AO and Fe_3O_4-OL.

2.2. Synthesis of silica-coated iron oxide samples

The two silica-coated samples were synthesized via Stöber method using tetraethyl orthosilicate (TEOS, 100 % VRW Chemicals) as silica coating agent [26]. These preparations were carried out starting from 0.02 g of each of the previously synthesized Fe_3O_4-AO and Fe_3O_4-OL samples (see reaction scheme Fig. 1.b). Initially, these powders were dispersed in two of the two-necked reaction flasks by adding a 4:1 ratio of EtOH:H_2O mixture. These reactions were carried out at room temperature with mechanical stirring under Ar atmosphere. In this reaction medium, ethanol provides the OH^- groups necessary to facilitate the adhesion of the polymeric network …O-Si-O-Si-O… to the dispersed particles of the considered sample. Next, 2 mL of NH_3 (32 %) was slowly added, which catalyzes the reactions. Then, 0.4 mL of TEOS was slowly added. After 24 hours, the resulting black powders were isolated by magnetic decantation and dried by heating at 50 °C for 3 hours and washed with hexane. The two samples obtained are named Fe_3O_4-AO@SiO_2 and Fe_3O_4-OL@SiO_2 [26].

2.3. Characterization techniques

The structural characterization of all synthetized samples was carried out by X-ray diffraction (XRD) employing a PANalytical XPERT-PRO diffractometer with Cu Kα radiation. For data collection, a step

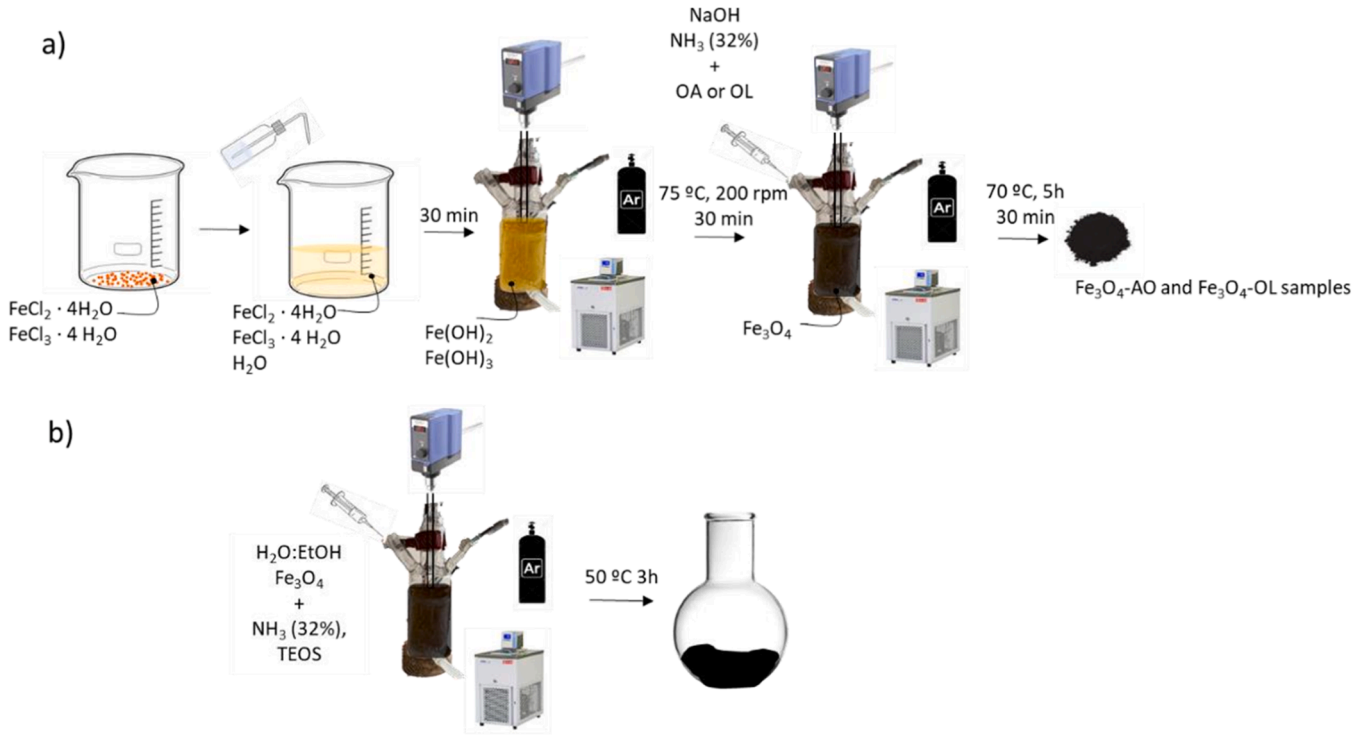

Fig. 1. (a) Scheme showing the synthesis process of the two magnetic samples. (b) Scheme showing the coating process of the two magnetic samples.

scan of 0.033° (2θ) was used in the ranges 10–70° and a counting time of 200 seconds for each step. The instrumental broadening of the diffraction peaks was considered and calibrated using the LaB6 standard NIST SRM 660b. Powder diffraction data were refined by the Rietveld method using the FullProf software [27,28]. A Thompson-Cox-Hastings function and a Lorentzian function were used to describe the XRD peak shape of Fe_3O_4-OL and Fe_3O_4-OA samples, respectively.

Infrared spectra of samples were recorded employing a FTIR spectrophotometer with attenuated total reflectance (ATR) between 450 and 4000 cm^{-1} and a resolution of 1 cm^{-1}. For measurements, the sample powders were pressed against a diamond

The morphological characterization of samples was performed considering the TEM images obtained in a transmission electron microscope operating at 200 kV and equipped with a field emission electron gun, providing a spot resolution of 0.19 nm. For measurement, the samples were dispersed in n-butanol and a drop of the resulting dispersions was deposited on a 300-mesh carbon-coated copper grid.

^{57}Fe Mössbauer data were recorded at different temperatures in the transmission mode using a conventional constant spectrometer, a ^{57}Co (Rh) source and a He closed-cycle cryorefrigerator. The absorbers were prepared to give an effective absorber thickness around 5 mg of natural iron/cm^2. The velocity scale was calibrated using a 6 μm thick α-Fe foil. The chemical isomer shifts were referred to the centroid of the α-Fe spectrum at room temperature.

The magnetic behavior of investigated samples has been studied measuring the magnetization (M) with the applied magnetic field (H) at room temperature. The hysteresis loops of the samples were measured at room temperature using a coercivities spectrometer and the field reached up to 50000 Oe [29].

Dynamic light scattering distribution and zeta potential of particles constituent of all samples were characterized with the Micrometrics NanoPlus particle size and zeta potential analyser. The isoelectric point was obtained by modifying the pH of the water dispersed samples by adding drops of 0.05 M HCl and 0.05 M NaOH solutions.

3. Results and discussion

3.1. X-ray diffraction

Comparative XRD patterns of uncoated and silica coated iron oxide samples are shown in Fig. 2. In all cases, XRD patterns show diffraction maxima that can be indexed to a cubic symmetry of space group $Fd\bar{3}m$ with Z = 8 [JCPDS card file nº 01–088–0315], compatible with an inverse spinel structure-type. Other diffraction maxima are not observed under the conditions used to record the XRD data, confirming the purity of synthetized samples.

In addition, a slightly lower intensity is observed in some diffraction maxima of the Fe_3O_4-OA sample, indicating that the presence of a different surfactant (oleic acid and oleylamine) does not influence the crystalline structure of the obtained samples.

A curve centered at 22° (in units of 2θ) confirming the presence of silica [30] is observed in the X-ray diffraction patterns of the two silica-coated samples. Furthermore, a lower intensity of diffraction maxima is observed in the profile of Fe_3O_4-OL@SiO_2 sample. This result can be explained by considering the silica shell thickness that can be homogeneously present in the environment of the constituent particles of the investigated samples, indicating a greater thickness of the silica shell in these sample, where the intensity of the most intense maximum is reduced from 630 to 380 arbitrary units.

When preparing magnetite iron oxide samples, it is very common to find that these samples may be slightly oxidized, and a certain proportion of the maghemite γ-Fe_2O_3 phase may be found in them. Since the lattice parameters of magnetite and maghemite phases are quite similar, and in both cases the most intense diffraction maxima overlap, it is difficult to evaluate their presence separately. For this reason, to determine whether the Fe_3O_4-OL and Fe_3O_4-OA samples were oxidized, the XRD data were analyzed by the Rietveld method using the FULLPROF program [27,28]. In the refinements carried out, it was considered that the two phases magnetite and maghemite were present in these samples. The aim was to determine in what proportion they were present in each case.

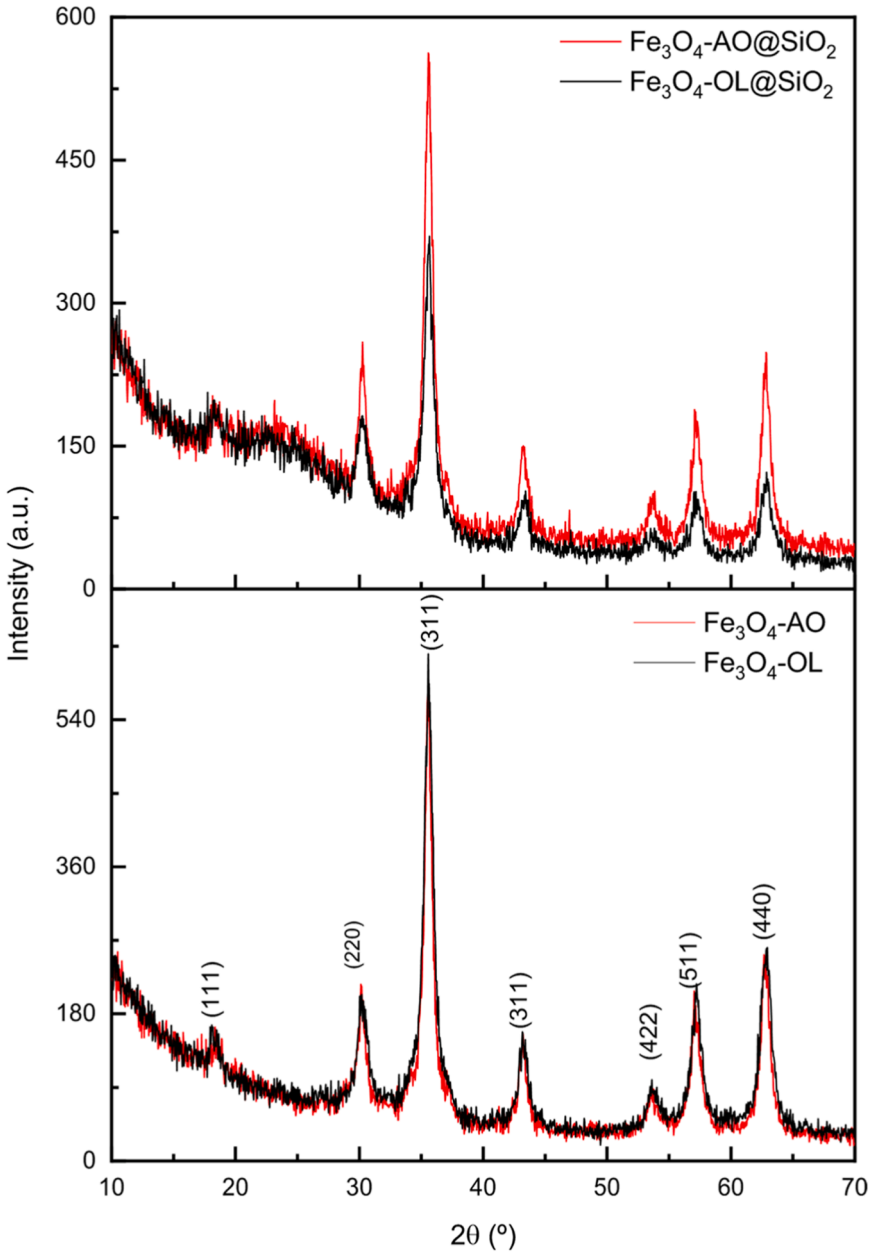

Fig. 2. XRD patterns of all investigated samples.

In these refinements, the magnetite phase was refined considering the structural parameters of a phase with cubic symmetry of space group $Fd\bar{3}m$ and Z = 8, compatible with an inverse spinel type structure. These refinements were carried out under two different assumptions which are reported in the literature. In the first case, iron atoms 1 and 2 were in the special positions 8a (1/8, 1/8, 1/8) and 16c (0, 0, 0), while the oxygen atoms in position 32e (x, x, x). In the second case, iron atoms 1 and 2 were in the special positions 8b (3/8, 3/8, 3/8) and 16d (0.5, 0.5, 0,5) and the oxygen atoms also in position 32e (x, x, x). The occupancy factors were defined based on the stoichiometry of the Fe_3O_4 composition considering the ratio between special positions and general positions. In these refinements, the best agreements were achieved according to the second assumption, i.e., by locating the Fe1 and Fe2 in the special positions 8b (3/8, 3/8, 3/8) and 16d (0.5, 0.5, 0.5) and the oxygen atoms in position 32e (x, x, x).

Based on the literature, for the refinement of the maghemite phase, two assumptions were also made. In the first case, a tetragonal symmetry of parameters a = 8.330 Å and b = 24,990 Å and space group $P4_12_12$ (92) [JCPDS card file nº004–0083650] was considered [31]. The iron atoms were in 8b and 4a positions and all oxygen atoms in 8b. In the second case, a cubic symmetry phase of parameter a = 8.3498 and space group $P4_332$ was considered [31,32]. The Fe1 atom was in the general octahedral position 12d (y + ½, y+1/4, 7/8), the Fe2 atom in the special octahedral position 4b (3/8, 1/8, 7/8) and the Fe3 atom and one of the oxygen atoms (O1) in the general position 8c (x, x, x) with x = 0.9947 and 0.8630, respectively.

Finally, the other oxygen atom (O2) apeears in the general position 24 e (x, y, z). Since cationic vacancies are present in the structure of maghemite, the existence of such vacancies in positions 8c, 4b and 12d was considered in the refinements. The best agreement factors R were obtained considering their presence in position 12d.

As an example, the observed, calculated and difference XRD patterns obtained in the refinements of the experimental XRD data of Fe_3O_4-OL and Fe_3O_4-OA samples are shown in Fig. 3. The atomic positions and the best refined *R*-factors obtained are summarized in Table 1.

The lattice parameters a = 8.3768(7) Å determined in Fe_3O_4-OL

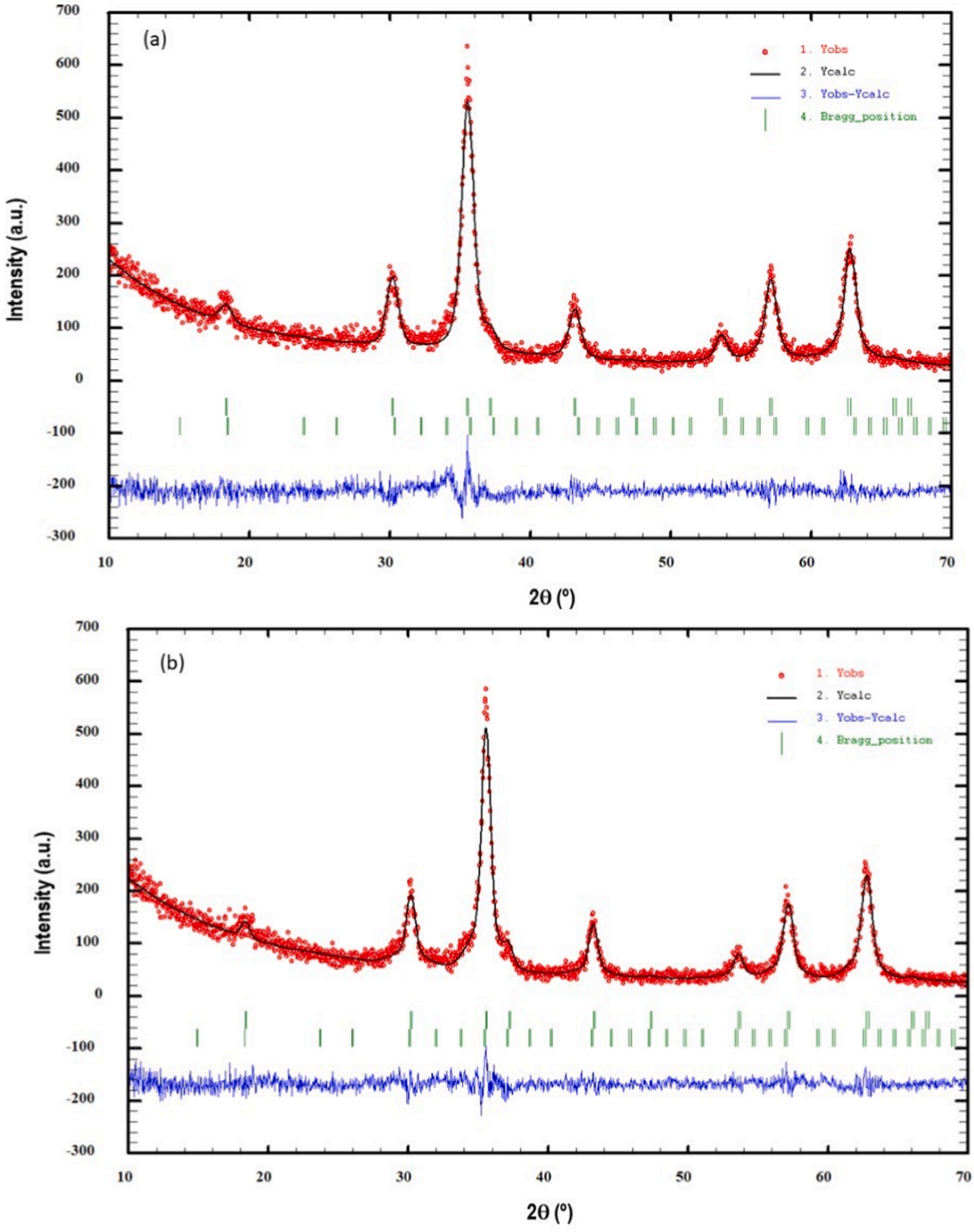

Fig. 3. Experimental (red line), calculated (black line) and difference (blue line) of XRD patterns of (a) Fe_3O_4OL and (b) Fe_3O_4-OA samples.

Table 1
Crystallographic parameters obtained in the refinements of Fe_3O_4 samples.

Fe_3O_4-OL					
Atom	x	y	z	Site	Occ.
Fe1	1/4	1/4	1/4	8a	0,25
Fe2	1/2	1/2	1/2	16d	0,5
O	0.2549 (2)	0.2549(2)	0.2549 (2)	32e	1
	Magnetite phase		Cubic S.G: Fd-3m (227)		a = 8.3768(7) Å
	R_p = 9,41	R_{wp} = 12,3	R_b = 6,6	R_f = 4.0	Percentage (%) = 88
Atom	x	y	z	Site	Occ.
Fe1	0.9955 (6)	0.9955(6)	0.9955 (6)	8c	0.333
Fe2	5/8	5/8	5/8	4b	0.167
Fe3	0.8650 (1)	0.6150(5)	7/8	12d	0.390
O1	0.1179 (1)	0.1297(4)	0,3809 (5)	24c	1
O2	0.8630 (1)	0.8630(1)	0.8630 (1)	8c	0.333
	Maghemite phase		Cubic S.G: $P4_332$ (212)		a = 8.3265(2) Å
	R_p = 30.3	R_{wp} = 27.4	R_b = 6,6	R_f = 6.7	Percentage (%) = 12
Fe-O(t_d)			4 × 1.8923(3)		
Fe-O(O_h)			6 × 2.0458 (3)		
Radii Shannon(Å): $Fe^{2+}(t_d)$ = 0.63; $Fe^{2+}(O_h)$ = 0.78; $Fe^{3+}(t_d)$ = 0.49					
Fe_3O_4-OA					
Atom	x	y	z	Site	Occ.
Fe1	1/4	1/4	1/4	8a	0.25
Fe2	1/2	1/2	1/2	16d	0.5
O	0.2524 (5)	0.2524(5)	0.2524 (5)	32e	1
	Magnetite phase		Cubic S.G: Fd-3m (227)		a = 8.3592(8) Å
	R_p = 10.3	R_{wp} = 13.2	R_b = 4.5	R_f = 3.6	Percentage (%) = 51
Atom	x	y	z	Site	Occ.
Fe1	0.9925 (5)	0.9925(5)	0.9925 (5)	8c	0.333
Fe2	5/8	5/8	5/8	4b	0.167
Fe3	0.8650 (1)	0.6150(3)	7/8	12d	0.390
O1	0.1179 (4)	0.1297(1)	0.3809 (1)	24c	1
O2	0.8480 (6)	0.8480(6)	0.8480 (6)	8c	0.333
	Maghemite phase		Cubic S.G: $P4_332$ (212)		a = 8.3265(2) Å
	R_p = 37.2	R_{wp} = 31.0	R_b = 13.6	R_f = 12.6	Percentage (%) = 49
	Fe-O(t_d)		4 × 1.892(1)		
	Fe-O(O_h)		6 × 2.045 (8)		

sample are very close to the theoretical value of iron oxide magnetite (a = 8.3750 Å), although the result of the refinement (see Table 1) shows a slight oxidation of the sample, confirming that around 12 % of the maghemite phase is present. This percentage increases in the Fe_3O_4-OA sample, 49 %, which is also confirmed considering the value of the "a" parameter determined in the magnetite phase that is closer to that of the maghemite phase (a = 8.3592(8) Å). However, it should be noted that, although the agreement factors are acceptable for the refinement of the magnetite phase in the two samples, they are not so acceptable for the maghemite phase. This fact is evident especially in the XRD refinement carried out for Fe_3O_4-OA sample (Fe_3O_4-OL: R_p = 30.3; R_{wp} = 27.4 and Fe_3O_4-OA: R_p = 37.2; R_{wp} = 31.0; R_b = 13.6; R_f = 12.6). For this reason and to be able to discern more safely the percentage of oxidation that these samples presented, they were studied using the technique of Mössbauer spectroscopy, as will be described later.

A perspective of the inverse spinel-type structure [33] present in these samples that was generated from Rietveld refinements is shown in Fig. 4. Fe^{2+}/Fe^{3+} ions are centered in their respective octahedral environment, and remanning Fe^{3+} ions show a fourfold coordination. Therefore, the Fe^{3+} ions occupy half of the tetrahedral sites, while the Fe^{2+} ions are distributed between the octahedral sites and the remaining tetrahedral sites. The structure can be described by [FeO_6] octahedra chains that share edges along the diagonals of the cube faces and that share vertices with [FeO_4] tetrahedra.

An estimation of the average crystalline size of synthetized samples was made (see Table 1) using the Scherrer formula [34]: $D_{hkl} = 0.89\lambda/\beta\cos\theta$ where D_{hkl} is the crystallite size (here determined from the (220), (311), (400) and (440) planes), 0.89 is the shape factor assuming spherical particles, θ is the Bragg's angle, β is the full-width at half-maximum (FWHM) of the experimental peaks and λ the X-ray wavelength (1.5418 Å). In all cases, nanoparticles of 50.09 and 42.87 Å have been found for Fe_3O_4-OA and Fe_3O_4-OL samples, respectively.

3.2. FTIR spectroscopy

FTIR spectra of all synthesized samples are shown in Fig. 5. In the spectra of Fe_3O_4-OL and Fe_3O_4-AO samples, a very strong intensity band is observed at 560 cm^{-1} which is assignable to the stretching vibration of the Fe-O bonds of cations that are in the tetrahedral positions of their spinel-related structure [26,35]. In the Fe_3O_4-OL spectrum, the very weak and broad band around 3300 cm^{-1} corresponds to the stretching vibrations of the $-NH_2$ group present in the oleylamine surfactant. This weak presence is also confirmed in the weak band at 591 cm^{-1} and assigned to the β(NH_2) scissoring mode, in agreement with that reported in pure oleylamine at 1593 cm^{-1}.

The weak bands at 2919 cm^{-1} and 2848 cm^{-1} in the spectra of Fe_3O_4-OL -and Fe_3O_4-AO samples are assigned to the asymmetric and symmetric stretching of CH_2 groups, in agreement with that reported at 2922 and 2854 cm^{-1} in both oleylamine and oleic acid pure. Its presence and weak intensity reveal the presence of oleic acid and of oleylamine residues in the samples, and its small wavenumber shift related to these surfactants indicates that the CH_2 groups of these residues have little interaction with the Fe_3O_4 core. Weak bands have been also observed at 1538 and 1516 cm^{-1} in the spectra of both samples that can be assigned to complex combinations of the ν(C-C) and ν(C-N) or $\nu_{as}(COO^-)$ modes. In the spectra of Fe_3O_4-OL sample appears also very weak bands at 1550 cm^{-1}, 1464 cm^{-1}, 1385 cm^{-1} that can be assigned to the asymmetric and symmetric deformation of the C-H bonds present in CH_2 groups, respectively [36].

In the spectrum of Fe_3O_4-AO samples, a broad band with medium intensity can be observed at 1406 cm^{-1} that can be assigned to the $\nu_{as}(COO^-)$ mode. Its lower wavenumber than the C═O stretch can be explained due to the carboxyl group interactions of oleic acid with the Fe atoms on the Fe_3O_4 nanoparticle surface, which weaken the C═O bond to a partial single bond character and shifting its stretching wavenumber to a lower value. Todorovsky et al. [37] proposed that the carboxyl groups of oleic acid are chemisorbed on the surface [38].

In the spectra of silica coated samples, the stretching ν(C-H) and bending δ(N-H) and δ(CH_2) bands disappear indicating that the oleic acid and oleylamine residues are not present in the samples. This feature and the appearance of new and strong bands corresponding to silica indicate a high effectiveness of the coating process. The very weak and broad bands observed at around 3300 cm^{-1} and 1630 cm^{-1} in the Fe_3O_4OL@SiO_2 spectrum can correspond to stretching and in-plane bending O-H modes, respectively, of very few hydrated water molecules present in this sample.

The most characteristic bands in the silica coated samples are those corresponding to the asymmetric and symmetric stretching vibrations of O-Si-O bonds and to the asymmetric stretching vibration of Si-O-Si bonds, which were well related to the bands observed at 1210 cm^{-1}, 795 cm^{-1} and 1065 cm^{-1}, respectively. The same band profile of these vibrations was found in related coated samples [26].

With the silica coating, the band at 560 cm^{-1} and assigned to the Fe-O stretching vibration of cations located in tetrahedral positions is

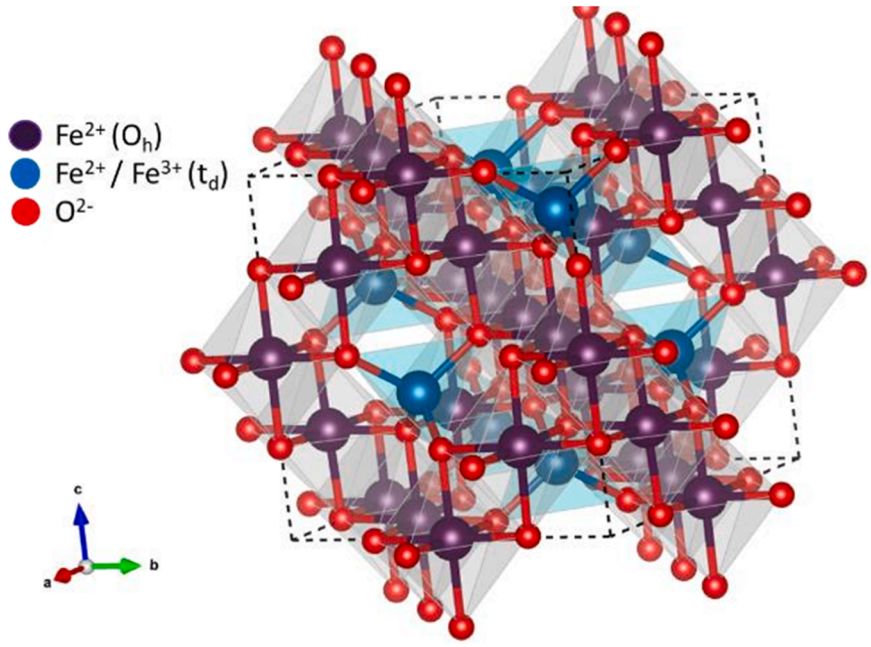

Fig. 4. Perspective in the cb plane of the structure of the investigated samples.

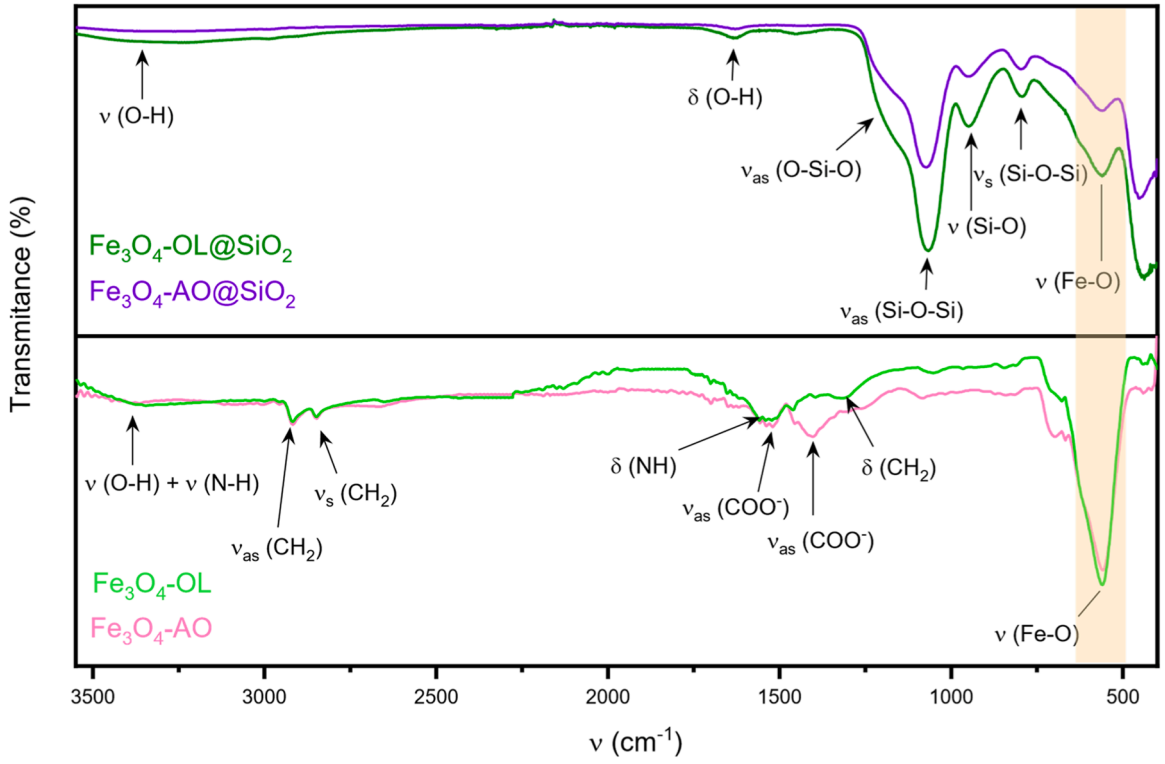

Fig. 5. FTIR spectra of investigated samples.

remarkable reduced in its intensity by the effectiveness of the coating process and it agrees with other authors [39].

3.3. Transmission Electron Microscopy (TEM)

TEM images of all synthesized samples are shown in Fig. 6. In all cases, spherical particles with relatively low aggregation are found, which seems to be lower in the Fe_3O_4-AO powder. The long-range magnetic dipole-dipole interaction between the magnetic nanoparticles may be the cause of the agglomeration visualized in these images, which probably originated in the drying process when preparing the samples for TEM images. The particle size distribution graphs also included, made by measuring at least 200 particles and using ImageJ software (National Institutes of Health, USA), show individual particles with a mean diameter of 7 ± 2 nm in the Fe_3O_4-OL sample image and of 9 ± 2 nm in that of Fe_3O_4-AO sample. It should be noted that the particle size is more homogeneous in the sample powder prepared by adding oleylamine. These values are different from those determined from the

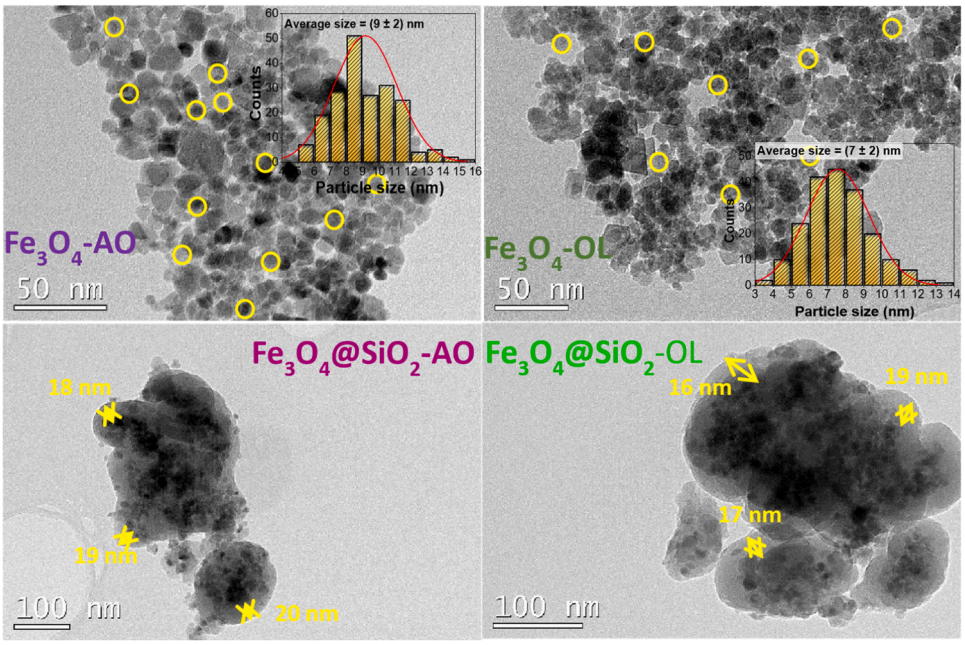

Fig. 6. TEM images of all synthetized magnetic samples.

XRD profiles in Fig. 1 (50.09 and 42.87 Å for Fe_3O_4-OA and Fe_3O_4-OL). It can be justified considering that what is determined by XRD is the average size of the crystalline domain, while Fig. 6 shows the high agglomeration degree of the particles in these samples.

The small difference in size and a greater or lesser homogeneity of the particles present in the two samples investigated can be explained by considering both the spatial distribution of the atoms and the different functional groups present in the surfactants added in the sample preparation [40].

Oleic acid is a monounsaturated fatty acid whose molecular chemical formula is $C_{18}H_{34}O_2$ or expanded, $CH_3(CH_2)_7CH{=}CH(CH_2)_7COOH$, while oleylamine is an unsaturated fatty amine related to the fatty oleic acid with a molecular formula $C_{18}H_{35}NH_2$ or expanded $CH_3(CH_2)_7CH{=}CH(CH_2)_7CH_2NH_2$. Our results show a smaller particle size and a greater homogeneity in the sample prepared with oleylamine, probably due to the different molecular structure of this surfactant and a higher adsorption capacity on magnetic nanoparticles suspended in a basic medium [41].

In the powder of the silica-coated samples, elongated silica pockets are observed that encompass nanoparticles and whose thickness is between 16 and 19 nm in the Fe_3O_4-OL@SiO_2 sample and between 16 and 20 nm in the Fe_3O_4-AO@SiO_2 sample. These results are similar to those we have found in previous research [15,30].

3.4. Mössbauer spectroscopy

In this work we have used this technique both at room and cryogenic temperatures to gather information on the nature of the different samples.

It is well-known [13,42,36,43] that the room temperature Mössbauer spectrum of bulk magnetite consists of two well-separated magnetic sextets: one corresponding to the Fe^{3+} ions sitting on the tetrahedral sites of the spinel-type structure, and a second corresponding to the Fe^{3+}/Fe^{2+} ions occupying the octahedral sites. These octahedral sites have hyperfine parameters characteristic of a mixed valence $Fe^{2.5+}$ species due to the occurrence of electron hopping between the Fe^{3+} and Fe^{2+} octahedral cations. In the case of magnetite nanoparticle samples, the spectra can look very different depending on the nature of the particles, their size, or their particle size distribution [13,42,36,43,44]. There is significant experimental evidence that the room temperature Mössbauer spectrum of non-interacting isolated magnetite nanoparticle samples of sizes below 10 nm consists of either a singlet or an asymmetric doublet [13,42,36]. This paramagnetic component can persist even down to 80 K for 5 nm magnetite particles [13]. In the case of larger particles (i.e. 15 nm or larger) the spectrum shows the two characteristic sextets of magnetite, although with broadened lines as compared with the bulk magnetite spectrum [13,45]. If the particles are not so well isolated and dipolar interparticle interactions become important, the spectra show very broad asymmetric lines [45]. Of course, surface effects can also play an important role as the particle size decreases. The situation becomes even more complicated if the nanoparticle distribution size is not narrow, since then many intermediate situations can coexist.

The particle size distributions determined in this work by TEM for the uncoated and silica-coated samples (see Fig. 6) are in the range 7–9 nm, extending even to values of 12 and 14 nm.

For this particle sizes, if the samples were composed of perfectly isolated noninteracting nanoparticles, one would expect a Mössbauer spectrum dominated by an intense central paramagnetic signal [13,42,36,43]. However, in all cases the spectra show (see Fig. 7) broad asymmetric magnetic patterns indicating that the situation appears to be much more complex. The spectra were fitted using two narrow sextets with parameters close to those shown by canonical magnetite (although with smaller hyperfine magnetic fields), together with a small paramagnetic doublet and a broad magnetic component. The average hyperfine parameters are collected in Table 2 and the respective relative areas of the different components are presented in Table 3.

This type of fit would account for a situation arising from: (a) the existence of a particle size distribution: the doublet corresponding to the smaller particles, the sharper sextets to the larger particles and the broad magnetic component to the rest of intermediate situations and, (b) the occurrence of dipolar interparticle interactions and/or other dynamic or surface interplay effects because, despite being covered by a surfactant, the nanoparticles in the present investigation appear to be not so well isolated as in other similar works [13,42,36]. They show some degree of agglomeration (see TEM micrographs, Fig. 6), which would support the presence of interparticle interactions. Inspection of Fig. 7 indicates that the differences among the spectra are not very large. One of these differences concerns the relative doublet area, which is significantly larger in the case of the silica-coated samples than in their uncoated

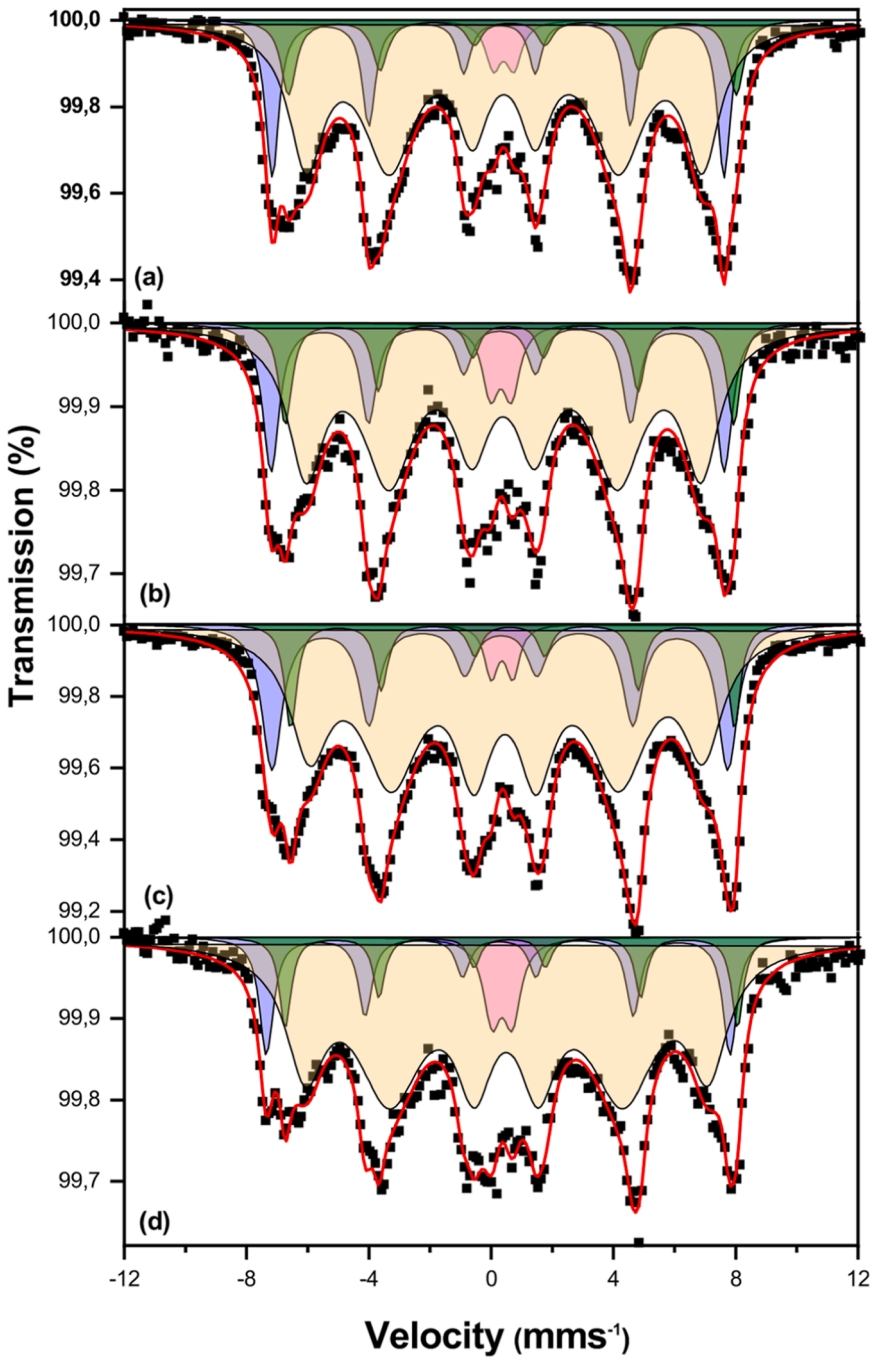

Fig. 7. - Room temperature Mössbauer spectra recorded from (a) Fe_3O_4-OL, (b) Fe_3O_4-OL@SiO_2, (c) Fe_3O_4-AO and (d) Fe_3O_4-AO@SiO_2.

Table 2
Average hyperfine parameters obtained from the fit of the RT spectra recorded from the different samples.

	Doublet	Sextet1	Sextet2	Sextet3
δ (mms^{-1}±0.02 mms^{-1})	0.36	0.26	0.63	0.46
Δ, 2ε (mms^{-1}±0.02 mms^{-1})	0.68	−0.05	0.07	0.02
H (T±0.3 T)	–	46.0	45.5	40.3

δ, isomer shift; Δ, quadrupole splitting (refers to doublets), 2ε, quadrupole shift (refers to sextets), H, hyperfine magnetic field.

Table 3.-
Relative areas of the various components used to fit the room temperature spectra recorded from the different samples.

Sample	Doublet	Sextet1	Sextet2	Sextet3
Fe_3O_4-OL	3	19	10	68
Fe_3O_4-OL@SiO_2	5	19	11	65
Fe_3O_4-AO	3	22	10	66
Fe_3O_4-AO@SiO_2	5	13	8	74

counterparts. It is also worth mentioning that the broad magnetic component is significantly more intense in the case of Fe_3O_4-AO@SiO_2 probably reflecting a more inhomogeneous particle size distribution as TEM has suggested.

The spectra recorded at 150 K (Fig. 8) show much better resolved magnetic patterns than those at room temperature, although the lines continue being asymmetric in their inner wings. Again, the spectra

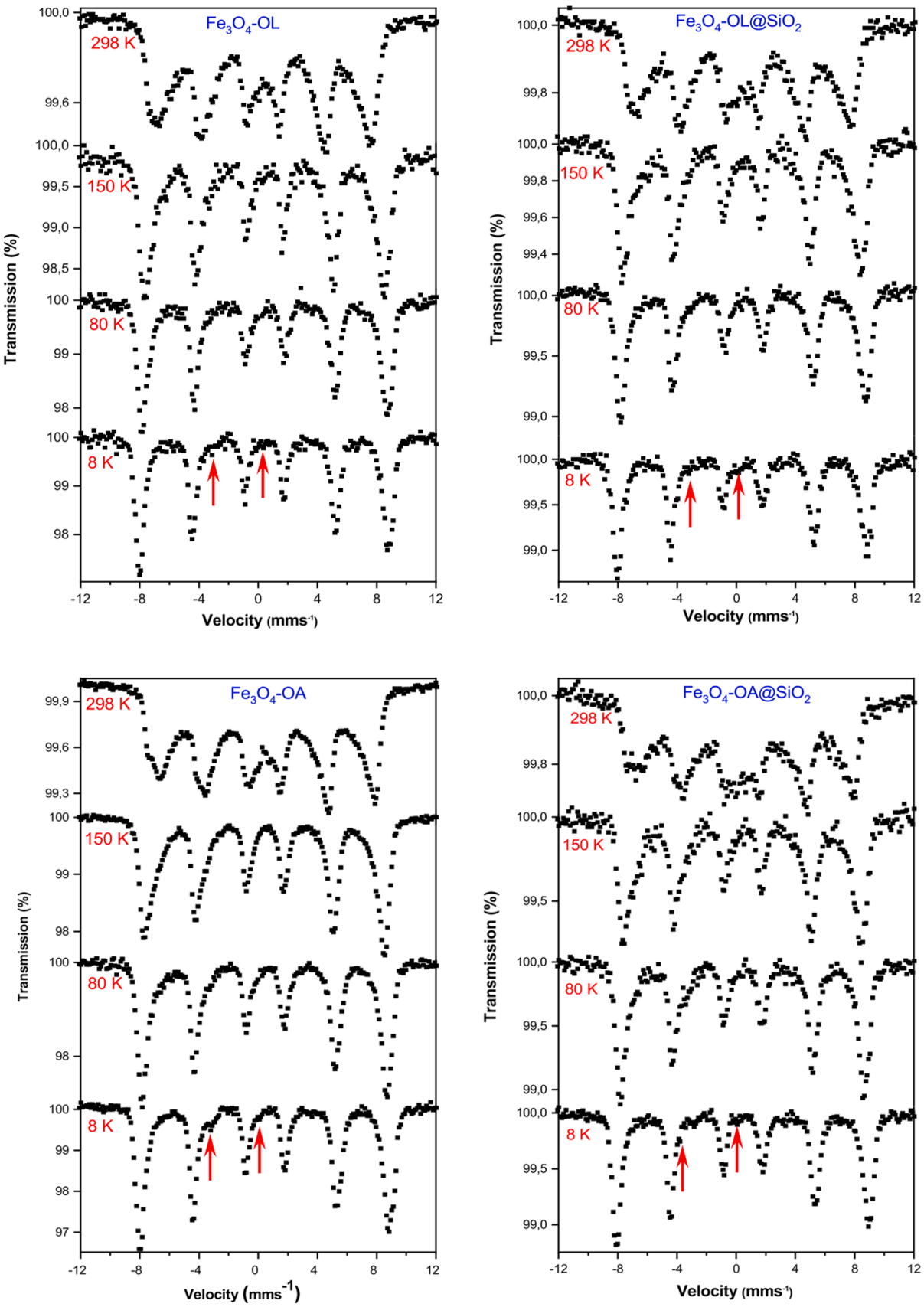

Fig. 8. - Mössbauer spectra recorded at different temperatures from the investigated samples.

contrast with those recorded from isolated magnetite nanoparticles of comparable sizes that show central paramagnetic components down to 80 K [13], something that is not observed here.

This would support the likely occurrence of magnetic interparticle interactions, as we have already suggested from the room temperature data.

It is known that at the Verwey transition magnetite suffers a phase transition, its structure passing from cubic to monoclinic [46–48]. The low temperature Mössbauer spectra of magnetite below the Verwey transition change accordingly and, instead of showing two sextets, they need to be fitted using four or five different sextets, corresponding to the various sites available for iron within the new structure [42,36,46,48]. Because of the large quadrupole interaction experienced by the octahedral Fe^{2+} ions sites, the spectra show very distinctive features at approximately −3.8 mms^{-1} and −0.5 mms. In the case of pure, stoichiometric bulk magnetite o magnetite single crystals, these features are very intense, while for magnetite nanoparticles, they are usually much less prominent. Since these features are related to the presence of Fe^{2+} ions, a decrease in their relative area is usually related to the occurrence of octahedral vacancies (i.e. to the occurrence of non-stoichiometry) and/or to the partial oxidation of magnetite to maghemite. Therefore, the determination of the relative area of these two Fe^{2+} components can be used to gather information about the non-stoichiometry/degree of oxidation of magnetite. Fig. 8 clearly shows the occurrence of the above-mentioned distinctive features in the 80 and 8 K spectra in all the samples (see the red arrows), which they seem to be more intense in the spectrum of the Fe_3O_4-AO sample.

To quantify the contribution of the Fe^{2+} ions sextets we fitted the 8 K spectra following the procedure outlined in [36,43], where four sextets are used, one accounting for tetrahedral Fe^{3+} ions, a second for

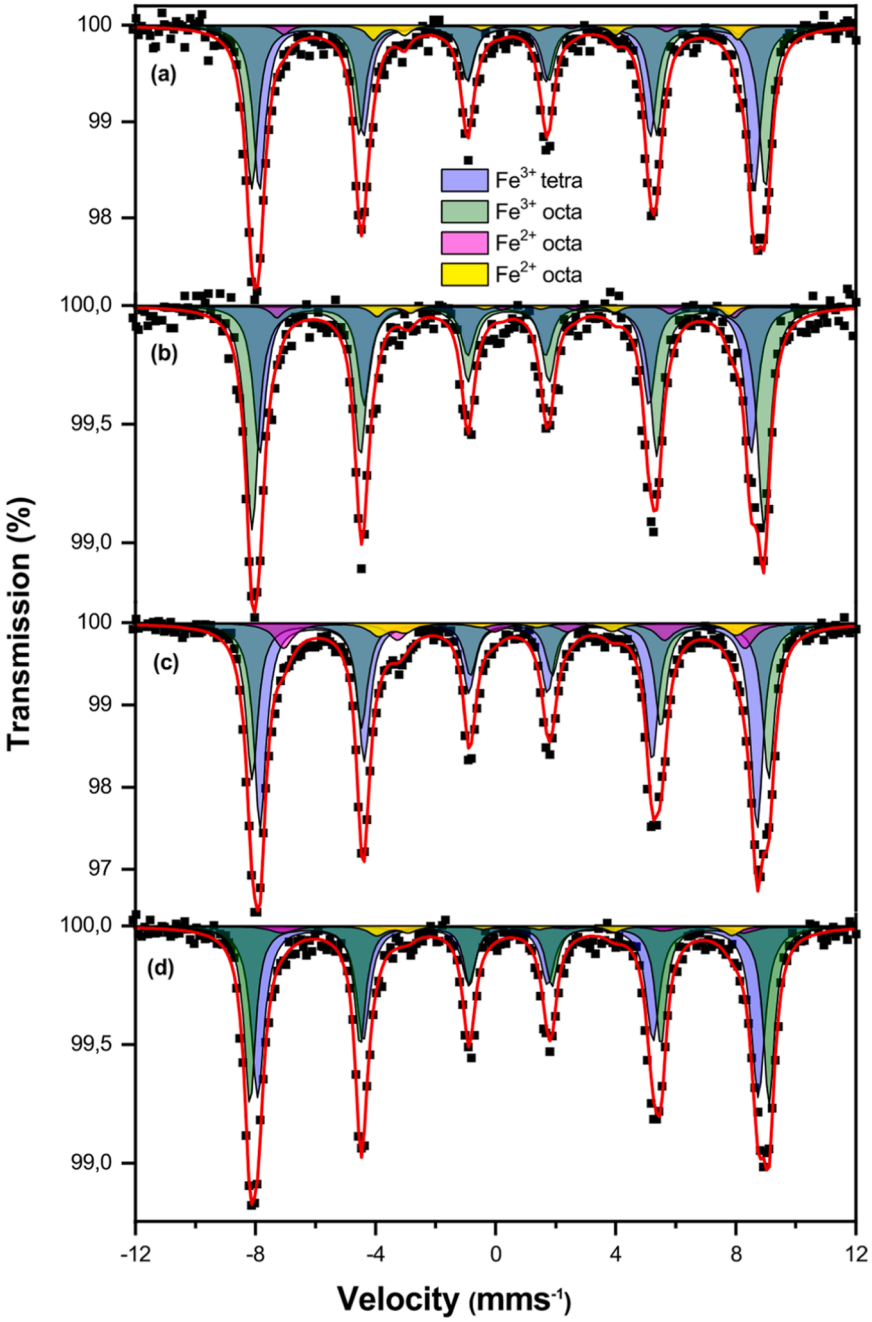

Fig. 9. - Mössbauer spectra recorded at 8 K from (a) Fe_3O_4-OL, (b) Fe_3O_4-OL@SiO_2, (c) Fe_3O_4-AO and (d) Fe_3O_4-AO@SiO_2.

octahedral Fe^{3+} ions and two additional for octahedral Fe^{2+} ions. These fits are shown in Fig. 9, the corresponding average hyperfine parameters appear in Table 4 and the respective relative areas in Table 5.

The 8 K Mössbauer results, which show Fe^{2+} percentages ranging between 6 % and 14 %, confirm that the samples correspond either to highly stoichiometric magnetite (a perfectly stoichiometric magnetite should contain a 25 % Fe^{2+}) or to a mixture of maghemite and magnetite. Although in the absence of an external applied magnetic field it is difficult to disentangle any possible concurrence of maghemite and (non-stoichiometric) magnetite we can perform some simple calculations to get an approximate idea on the nature of the samples. Non-stoichiometric magnetite can be formulated as [36,42]:

$$[Fe^{3+}]_A[Fe^{2+}_{1-3\delta}Fe^{3+}_{1+2\delta}]_B O_4$$

where δ is the non-stoichiometry parameter, which can vary between 0.00 and 0.33. In the case of δ = 0.33 the formula corresponds to maghemite (γ-Fe_2O_3), which is the end-ofseries of non-stoichiometric magnetite [49].

If R is the Fe^{3+}/Fe^{2+} ratio, the non-stoichiometry parameter is given by:

$$\delta = \frac{R-2}{3R+2}$$

According to this equation and considering the relative areas given in Table 5, we obtain that the non-stoichiometric parameter is 0.27, 0.28, 0.20 and 0.27 for Fe_3O_4-OL, Fe_3O_4-OL@SiO_2, Fe_3O_4-OA and Fe_3O_4-OA@SiO_2, respectively.

These numbers indicate that the present samples correspond, as suspected, to highly non-stoichiometric magnetite. As mentioned above, without an external applied field it is very difficult to separate any maghemite/non-stoichiometric magnetite contributions. Thus, the possibility that the samples are also partly oxidized to maghemite cannot be ruled out, although its contribution cannot be determined with precision from these Mössbauer measurements. In any case, the Mössbauer data clearly indicate that three of the samples have very similar Fe^{2+} contents, while the Fe_3O_4-AO sample has twice those Fe^{2+} concentrations. It is important to mention that, despite the difficulties in separating the possible maghemite/magnetite contributions, Mössbauer spectroscopy is able to identify the presence of Fe^{2+} in the 8 K spectra quite reliably.

This is because the large isomer shifts, the very large quadrupole shifts, and the small hyperfine magnetic fields make the Fe^{2+} components to be significantly separated from the Fe^{3+} sextets. Consequently, the Fe^{2+} concentration can be quantified with sufficient confidence. In this sense, Mössbauer spectroscopy is superior to other techniques such as XRD whose complications in unequivocally identifying magnetite from maghemite are well known.

3.5. Magnetic behaviour study

The magnetic field dependence of magnetization at room temperature of all obtained samples is shown in Fig. 10, while the magnetic parameters determined from these sigmoid curves is summarized in Table 6.

All Fe_3O_4 samples show a practically superparamagnetic behavior with very low coercive fields (H_c = 6.5–1) and remanent magnetization, M_r, between 0.709 and 0.176 Oe for Fe_3O_4-OL and Fe_3O_4-AO samples, respectively. The lower H_c value in the sample could be justified by a lower degree of the agglomeration of the particles of sample, as observed in the TEM images. In any case, all H_c and M_r values indicate that these samples may be useful in biomedicine as systems that show the ability to respond quickly and effectively to the presence of an external magnetic field.

As in previous investigations that we have carried out in other magnetic ferrite samples [15,22], M_s values of 64.30 and 62.26 emu/g determined in Fe_3O_4-OL and Fe_3O_4-AO samples, respectively, are lower than the theoretical value of magnetite or maghemite in bulk (92 emu/g and 78 emu/g, respectively [50,51]), being slightly lower in the sample that was prepared with OA. These results can be explained considering the nanometric size of particles in the investigated samples, which has been confirmed by transmission electron microscopy. The net magnetization value is influenced by the magnetic spin contributions on the particle surface, which are not aligned in the same direction as the applied magnetic field, thus decreasing the experimental value of the theoretical one value. This influence increases in nanoparticles due to their high surface area per unit volume that increases the number of spins that are aligned in the field direction causing this reduction in the magnetization values [51]. Furthermore, it can be observed that the saturation magnetization M_S is reduced in the silica-coated samples because of the non-magnetic silica coating that covers the particles.

This effect agrees with what we have already published in other works [15,26,30,52,53], being slightly higher in the samples prepared with OL (64.3 - 30.69 = 33.61 emu/g vs. 62.26 - 29.92 = 32.34 emu/g for samples prepared with OA).

As can be seen, both the uncoated and silica-coated samples show superparamagnetism and higher saturation magnetization even than those reported by us in previous works [15,22]. For this reason, it will be necessary to address the study of their stability when these samples suspended in a specific medium.

Table 4.-
Average hyperfine parameters obtained from the fit at 8 K spectra recorded from the different samples.

	Doublet	Sextet1	Sextet2	Sextet3
δ (mms^{-1}±0.02 mms^{-1})	0.39	0.46	0.89	1.24
Δ, 2ε (mms^{-1}±0.02 mms^{-1})	−0.01	−0.03	−0.75	1.48
H (T±0.3 T)	51.2	53.2	47.4	36.9

δ, isomer shift; Δ, quadrupole splitting (refers to doublets), 2ε, quadrupole shift (refers to sextets), H, hyperfine magnetic field.

Table 5.-
Relative areas of the various components used to fit the 8 K spectra recorded from the different samples.

SAMPLE	Fe^{3+}(tetra)	Fe^{3+} (octa)	Fe^{2+} (octa)	Fe^{2+} (octa)
Fe_3O_4-OL	47	46	4	3
Fe_3O_4-OL@SiO_2	38	57	3	3
Fe_3O_4-AO	49	37	9	5
Fe_3O_4-AO@SiO_2	49	44	4	3

3.6. Zeta potential and Dynamic Light Scattering (DLS) results

The potential use in biomedicine of the investigated samples will mostly depend on their stability when suspended in a specific medium. This stability will be clearly influenced by the presence or absence of the silica coating which, in turn, can affect the aggregation capacity of magnetic nanoparticles.

When a set of particles is suspended in a solvent, a diffuse electrical double layer is created on the surface that can attract counterions. Fig. 11 shows the zeta potential variation at pH values between 2 and 10. This representation allows us to determine the isoelectric point at which the zeta potential is zero. The variations observed in the graphs of Fig. 11 can be justified considering that the charge variation of nanoparticles of Fe_3O_4-OL and Fe_3O_4-OA samples is due to the Fe-OH_2^+ and Fe-O^- ions formation originated from Fe-OH groups [54,55]. This formation occurs in both acidic and basic medium. For Fe_3O_4-OA and Fe_3O_4-OL samples, the isoelectric point is reached at pH = 3.0 and at 5.3, respectively.

These values are similar to those described in other works for this type of samples [39,56] and are indicative of the better stability in water of the particles of Fe_3O_4-OA sample with respect to those of Fe_3O_4-OL. This better stability can be explained as due to the presence of acid

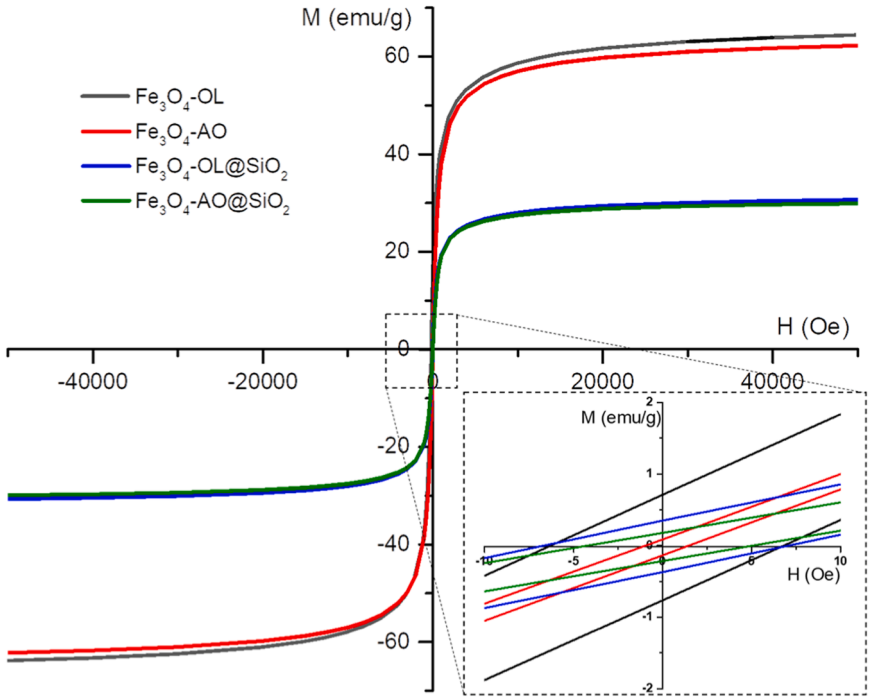

Fig. 10. M vs. H variation at room temperature of investigated samples.

Table 6
Magnetics parameters of prepared samples.

Sample	M_s (emu/g)	M_r (emu/g)	H_c (Oe)
Fe_3O_4-OL	64.30	0.709	6.5
Fe_3O_4-OL@SiO_2	30.69	0.349	7
Fe_3O_4-AO	62.26	0.176	1
Fe_3O_4-AO@SiO_2	29.92	0.177	4.5

groups (OH and -COOH) on the particle surface of Fe_3O_4-OA sample that also leads to a wide range of negative values of the zeta potential throughout the pH range studied. Contrarily, the change in the isoelectric point of the Fe_3O_4-OL sample can be justified by the presence of amino groups on the particle surface [57].

Fig. 11 also shows more negative zeta potential values of silica-coated samples in basic medium with respect to those shown by uncoated samples. The isoelectric point values determined for Fe_3O_4-OL@SiO_2 and Fe_3O_4-OA@SiO_2 samples are reached at pH values of = 3.8 and 2.1, respectively, being lower than in uncoated samples.

These values are similar to those described in other works for this

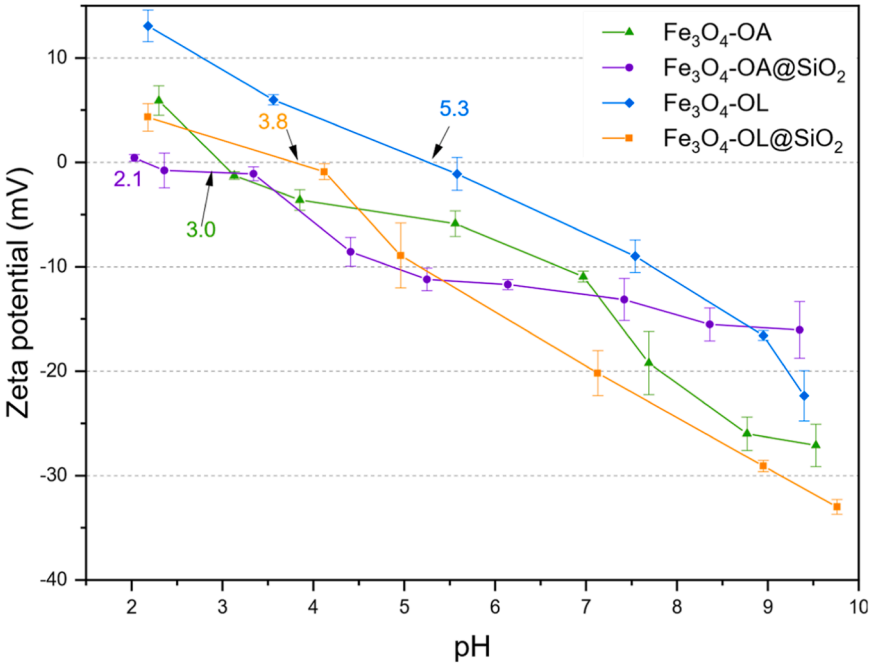

Fig. 11. Zeta potential variation at different pH values of investigated samples dispersed in distilled water.

type of samples [39] and can be explained by considering the protonation and deprotonation of Si-OH bonds, and COOH and NH_2 groups present on the nanoparticle surface of these samples, as it has been confirmed from the study of the FTIR spectra (see Fig. 5). Likewise, the presence of a higher number of negatively charged Si-OH groups [55] could justify the higher value of the isoelectric point determined for the Fe_3O_4-OL@SiO_2 sample. For dispersibility purposes of the investigated samples in water, it is known that samples that reach a zeta potential between ±30 and ±40 mV, at a given pH, have good stability in that solvent [56].

Comparing the zeta potential values at neutral pH, in Fig. 11 can be seen that they are higher in the coated samples due to the presence of the silica layer on the NPs surface. Consequently, it should be noted that the most suitable for dispersibility purposes are the coated ones and, specifically, the best is the Fe_3O_4-OL@SiO_2 sample (at pH = 9-10 values the zeta potential are found between ±30 and ±40 mV).

The dispersibility of nanoparticles will always be influenced by the nature of the solvent. Rafael O. da Silva et al. [58] reported that tetrahydrofuran (THF) can act as a hydrogen bond acceptor in stable colloidal dispersions of OA and OL molecules containing carboxylic acids and primary amines. Comparatively, in this work the behavior of the investigated samples has been studied both in a polar solvent (H_2O) and in an organic and aprotic solvent such as THF, which shows greater affinity for the carboxylic and amino groups present on the surface of the magnetic nanoparticles [59]. The synthesized powders were dispersed in distilled water at physiological pH (≈7.5) and in THF. Fig. 12 shows the variation between the normalized intensity distribution and the average hydrodynamic diameter of the investigated samples after their dispersion.

Two wide average hydrodynamic diameter distributions can be

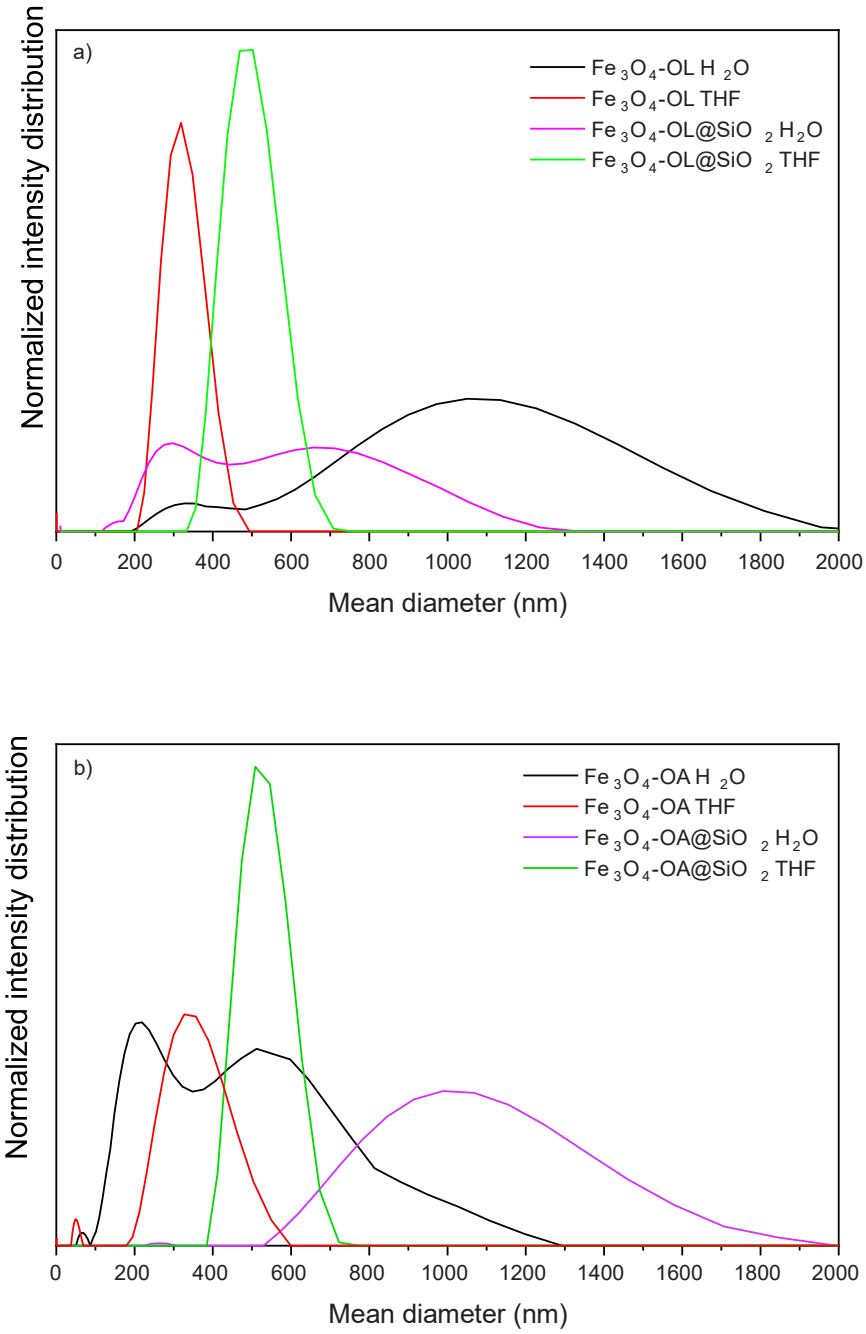

Fig. 12. Intensity distribution vs. hydrodynamic mean diameter of (a) the oleylamine samples and (b) the oleic acid samples dispersed in distilled water and THF.

observed for water dispersed samples, while only one narrow uniform size distribution is obtained in the THF dispersed ones. This result can be justified considering that THF is an organic and aprotic solvent that can more easily solubilize the carboxylic, amino and silanol groups present on the particle surface of investigated samples. From the graphs shown in Fig. 12, it is possible to determine the hydrodynamic diameter of the particles. This parameter is related to the amount of light that the particles can scatter when the samples are in suspension. Table 7 shows the average values of the hydrodynamic diameter and the polydispersity index.

The dispersion of samples in both water and THF leads to hydrodynamic sizes values that are in good agreement with that described in the literature [39,57,58]. However, these values are higher than the mean particle average size determined in the TEM images (see Fig. 6). This is because these values depend not only on the diameter of the particles but also on the concentration and type of ions present in the surrounding medium, while the TEM micrographs show the image of the dry powder once deposited on the grid [57].

Table 7 also shows that when Fe_3O_4-OL@SiO_2 and Fe_3O_4-AO samples are dispersed in water, lower PDI values are obtained than in the Fe_3O_4-AO@SiO_2 and Fe_3O_4-OL samples. A result that is in good agreement with the zeta potential values determined in Fig. 11 and that indicates its better dispersibility in water [57]. However, when all samples are dispersed in THF, all determined PDI values are much lower than those obtained when dispersing them in water, thus confirming their better stability and dispersibility in THF. In these last graphs of Fig. 12, larger diameter size values are also observed in our coatings, which can be justified by the silica layer that surrounds the magnetic NPs.

4. Conclusions

In the search of samples for medical applications, Fe_3O_4-OL, Fe_3O_4-OA, Fe_3O_4-OL@SiO_2, Fe_3O_4-OA@SiO_2 samples were successfully obtained by coprecipitation synthesis with oleylamine or oleic acid addition and subsequent reaction with TEOS. X-ray diffraction patterns confirm the inverse spinel-type structure of the synthesized uncoated samples, in good agreement with FTIR spectra. Particles of spherical morphology with a certain degree of agglomeration and a mean diameter of 7 and 9 nm were found in the TEM images of Fe_3O_4-OL and Fe_3O_4-AO samples, respectively. Elongated silica pockets whose thickness is between 16 and 19 nm were observed to encompass nanoparticles of the silica-coated samples. The Mössbauer results indicate that the samples consist mainly of non-stoichiometric magnetite having different stoichiometry degrees. In absence of applied magnetic field it is difficult to disentangle possible concomitant contributions of maghemite and non-stoichiometric magnetite. Taking this into account, the Mössbauer spectra recorded at 8 K suggest that the sample Fe_3O_4-AO is the one containing a larger proportion of magnetite as the area of the Fe^{2+} sextets is the highest of all the four studied samples. From the Mössbauer point of view, the remaining samples are much more non-stoichiometric/oxidized than this sample. In fact, the 8 K Mössbauer spectra recorded from these three samples are very similar, suggesting that the differences observed in their room temperature Mössbauer spectra must be more related to differences in their particle size distributions than to compositional variations. Another evidence from the Mössbauer results is that the present samples behave more similarly to systems composed of magnetically interacting particles than to systems composed of well-isolated, non-interacting nanoparticles. This appears to be supported by the TEM results if they are compared with those reported in the literature from similar related systems. In all cases, the determined Ms values are lower than the theoretical value of magnetite, being slightly higher in the samples prepared with OL. On the contrary, the lower Hc values of samples prepared with OA confirm their better superparamagnetic behavior. Higher negative zeta potential and lower PDI values are found in Fe_3O_4-AO@SiO_2 and Fe_3O_4-OL samples, indicating their better dispersibility in the solvent. When all samples are dispersed in THF, the PDI values are much lower than those obtained when dispersing them in water, confirming their better stability and dispersibility in THF.

Table 7
Mean hydrodynamic size and polydispersity index (PDI) values.

Sample	Mean hydrodynamic size (nm)	PDI
Fe_3O_4-OA H_2O	376 ± 324	0.49 ± 0.03
Fe_3O_4-OA @SiO_2 H_2O	1627 ± 481	0.59 ± 0.02
Fe_3O_4-OL H_2O	787 ± 516	0.67 ± 0.03
Fe_3O_4-OL@SiO_2 H_2O	492 ± 328	0.516 ± 0.009
Fe_3O_4-AO THF	252 ± 168	0.19 ± 0.01
Fe_3O_4-OA @SiO_2 THF	555 ± 106	0.21 ± 0.01
Fe_3O_4-OL THF	327 ± 78	0.23 ± 0.02
Fe_3O_4-OL@SiO_2 THF	535 ± 117	0.20 ± 0.02

CRediT authorship contribution statement

J.F. Marco: Writing – original draft, Investigation. **M. Rapp:** Writing – original draft, Visualization, Methodology, Investigation. **M. Alcolea Palafox:** Writing – review & editing, Writing – original draft, Visualization, Validation, Supervision, Methodology, Investigation. **Esther Hernán García:** Writing – original draft, Visualization, Methodology, Investigation, Conceptualization. **J. Isasi:** Writing – review & editing, Writing – original draft, Visualization, Validation, Supervision, Methodology, Investigation.

Declaration of Competing Interest

The authors declare the following financial interests/personal relationships which may be considered as potential competing interests: J. Isasi reports financial support was provided by Complutense University of Madrid. J. Isasi reports a relationship with Complutense University of Madrid that includes: board membership. If there are other authors, they declare that they have no known competing financial interests or personal relationships that could have appeared to influence the work reported in this paper.

Data availability

No data was used for the research described in the article.

Acknowledgements

This work was financially supported by the Spanish Ministry of Science and Innovation, through projects PID2019–106211RB-I00.

References

[1] C.D. Constantinescu, L.G. Petrescu, Magnetic materials, thin films and nanostructures, Magnetochem 9 (5) (2023) 133, https://doi.org/10.3390/magnetochemistry9050133.
[2] J.I. Mart, J. Nogu, K. Liu, J.L. Vicent, I.K. Schuller, Ordered magnetic nanostructures: fabrication and properties, J. Magn. Magn. Mater. 256 (1–3) (2003) 449–501, https://doi.org/10.1016/S0304-8853(02)00898-3.
[3] G. Guisbiers, S. Mejía-Rosales, F. Leonard Deepak, Nanomaterial properties: Size and shape dependencies, J. Nanomat. 2012 (2012), https://doi.org/10.1155/2012/180976.
[4] I. Khan, K. Saeed, I. Khan, Nanoparticles: properties, applications and toxicities, Arab. J. Chem. 12 (7) (2019) 908–931, https://doi.org/10.1016/j.arabjc.2017.05.011.
[5] N.A. Frey, S. Peng, K. Cheng, S. Sun, Magnetic nanoparticles: synthesis, functionalization, and applications in bioimaging and magnetic energy storage, Chem. Soc. 38 (9) (2009) 2532–2542, https://doi.org/10.1039/B815548H.
[6] D. Lisjak, A. Mertelj, Anisotropic magnetic nanoparticles: a review of their properties, syntheses and potential applications, Prog. Mater. 95 (2018) 286–328, https://doi.org/10.1016/j.pmatsci.2018.03.003.
[7] S. Singamaneni, V.N. Bliznyuk, C. Binek, E.Y. Tsymbal, Magnetic nanoparticles: recent advances in synthesis, self-assembly and applications, J. Mater. Chem. 21 (2011) 16819–16845, https://doi.org/10.1039/C1JM11845E.

[8] B.R. Ong, N.K. Devaraj, M. Matsumoto, M.H. Abdullah, Thermal stability of magnetite (Fe_3O_4) nanoparticles, Mater. Res. Soc. 1118 (309) (2008) 56–62, https://doi.org/10.1557/proc-1118-k03-09.

[9] U. Jeong, X. Teng, Y. Wang, H. Yang, Y. Xia, Superparamagnetic colloids: controlled synthesis and niche applications, Adv. Mater. 19 (1) (2007) 33–60, https://doi.org/10.1002/adma.200600674.

[10] M.D. Nguyen, H.V. Tran, S. Xu, T.R. Lee, Fe_3O_4 nanoparticles: Structures, synthesis, magnetic properties, surface functionalization, and emerging applications, Appl. Sci. 11 (23) (2021), https://doi.org/10.3390/app112311301.

[11] F.L. Deepak, et al., A systematic study of the structural and magnetic properties of Mn-, Co-, and Ni-doped colloidal magnetite nanoparticles, J. Phys. Chem. C. 119 (21) (2015) 11947–11957, https://doi.org/10.1021/acs.jpcc.5b01575.

[12] L. Blaney, Magnetite (Fe_3O_4): properties, synthesis, and applications, Lehigh Rev. 15 (2007) 5. ⟨http://preserve.lehigh.edu/cas-lehighreview-vol-15/5⟩.

[13] A.G. Roca, J.F. Marco, M.Del Puerto Morales, C.J. Serna, Effect of nature and particle size on properties of uniform magnetite and maghemite nanoparticles, J. Phys. Chem. C. 111 (50) (2007) 18577–18584, https://doi.org/10.1021/jp075133m.

[14] M. Coduri, et al., Local structure and magnetism of Fe_2O_3 maghemite nanocrystals: the role of crystal dimension, Nanomaterials 10 (5) (2020), https://doi.org/10.3390/nano10050867.

[15] P. Arévalo, J. Isasi, A.C. Caballero, J.F. Marco, F. Martín-Hernández, Magnetic and structural studies of Fe_3O_4 nanoparticles synthesized via coprecipitation and dispersed in different surfactants, Ceram. Int. 43 (13) (2017) 10333–10340, https://doi.org/10.1016/j.ceramint.2017.05.064.

[16] J.S. Bharti, S.S. Jangwan, Kumar, *et al.,* A review on the capability of zinc oxide and iron oxides nanomaterials, as a water decontaminating agent: adsorption and photocatalysis, Appl. Water Sci. 12 (46) (2022), https://doi.org/10.1007/s13201-02101566-3.

[17] A.V. Karim, Y. Jliao, M. Zhou, P.V. Nidheesh, Iron based persulfate activation process for environmental decontamination in water and soil, Chemosphere 265 (2021) 129057, https://doi.org/10.1016/j.chemosphere.2020.12905.

[18] A.V. Samrot, C.S. Sahithya, J. Selvarani A, S.K. Purayil, P. Ponnaiah, A review on synthesis, characterization and potential biological applications of superparamagnetic iron oxide nanoparticles, Curr. Res. Green. Sustain. Chem. 4 (2021) 100042, https://doi.org/10.1016/j.crgsc.2020.100042.

[19] P.L. Hariani, M. Faizal, R. Ridwan, M. Marsi, D. Setiabudidaya, Synthesis and properties of Fe_3O_4 nanoparticles by co-precipitation method to removal procion dye, Int. J. Environ. Sci. Dev. 4 (3) (2013) 336–340, https://doi.org/10.7763/ijesd.2013.v4.366.

[20] A.-G. Niculescu, C. Chircov, A.M. Grumezescu, Magnetite nanoparticles: synthesis, Methods- A Comp. Rev., Methods 199 (2022) 16–27, https://doi.org/10.1016/j.ymeth.2021.04.018.

[21] S.E. Favela-Camacho, E.J. Samaniego-Benítez, A. Godínez-García, L. M. AvilésArellano, J.F. Pérez-Robles, How to decrease the agglomeration of magnetite nanoparticles and increase their stability using surface properties, Colloids Surf. A Physicochem. Eng. Asp. 574 (2019) 29–35, https://doi.org/10.1016/j.colsurfa.2019.04.016.

[22] M. Rapp, Y. Lozano, M. Fernández-Ramos, J. Isasi, M.A. Palafox, Superparamagnetic and light-emitting bifunctional nanocomposites of iron oxide and erbium or thulium doped yttrium orthovanadate, J. Alloy. Compd. 929 (2022) 167065, https://doi.org/10.1016/j.jallcom.2022.167065.

[23] C. Cano-Sarmiento, D.I. Téllez Medina, R. Viveros-Contreras, M. Cornejo-Mazón, C. Y. Figueroa-Hernández, E. García Armenta, L. Alamilla-Beltrán, H.S. García, G. F. Gutiérrez-López, Zeta potential of food matrices, Food Eng. Rev. 10 (3) (2019) 113138, https://doi.org/10.1007/s12393-018-9176-z.

[24] J. Isasi, P. Arévalo, E. Martin, F. Martín-Hernández, Preparation and study of silica and APTES–silica-modified $NiFe_2O_4$ nanocomposites for removal of Cu^{2+} and Zn^{2+} ions from aqueous solutions, J. Solgel Sci. Technol. 91 (3) (2019) 596–610, https://doi.org/10.1007/s10971-019-05067-3.

[25] Y. Lu, X. Lu, B.T. Mayers, T. Herricks, Y. Xia, Synthesis and characterization of magnetic Co nanoparticles: a comparison study of three different capping surfactants, J. Solid State Chem. 181 (7) (2008) 1530–1538, https://doi.org/10.1016/j.jssc.2008.02.016.

[26] M. Fernández-Ramos, J. Isasi, M. Alcolea, T. Muñoz-Ortiz, E. Ortiz-Rivero, New magnetic-fluorescent bifuntional ($Y_{0.9}Ln_{0.1}VO_4/Fe_3O_4$)@$SiO_2$ and [($Y_{0.9}Ln_{0.1}VO_4$@SiO_2)/Fe_3O_4@SiO_2] materials, Ceram. Int. 48 (15) (2022) 22047–22058, https://doi.org/10.1016/j.ceramint.2022.04.191.

[27] J. Rodríguez-Carvajal, FULLPROF: a program for Rietveld refinement and pattern matching analysis. En Abstract of the Satellite Meeting of the XVth Congress of the International Union of Crystallography, University Paul Sabatier, Toulouse, Toulouse, France, 1990.

[28] T. Roisnel, J. Rodriguez-Carvajal. WinPLOTR. plotr@llb.saclay.cea.fr. ⟨http://wwwllb.cea.fr/fullweb/winplotr/winplotr.html⟩.

[29] P. Jasonov, D. Nougaliev, B. Burov, F. Heller, A modernized coercitivity spectrometer, Geol. Carpath. 49 (1998) 224–225.

[30] P. Arévalo-Cid, J. Isasi, F. Martín-Hernández, Comparative study of core-shell nanostructures based on amino-functionalized Fe_3O_4@SiO_2 and $CoFe_2O_4$@SiO_2 nanocomposites, J. Alloy. Compd. 766 (2018) 609–618, https://doi.org/10.1016/j.jallcom.2018.06.246.

[31] A.M. Escobaro, L.R. Pizzioa, G.P. Romanelli, Magnetic catalysts based on Iron Oxides: Synthesis, Properties and Applications, Ciencia en desarrollo 10 (1) (2019) 0121–7488, https://doi.org/10.19053/01217488.v10.n1.2019.88111.

[32] Z. Somogyvári, E. Sváb, G. Mészáros, K. Krezhov, I. Nedkov, I. Sajó, F. Bourée, Vacancy ordering in nanosized maghemite from neutron and X-ray powder diffraction, Appl. Phys A 74 (2002) S1077–S1079, https://doi.org/10.1007/s003390101192.

[33] W. Wu, Z. Wu, T. Yu, C. Jiang, W.S. Kim, Recent progress on magnetic iron oxide nanoparticles: synthesis, surface functional strategies and biomedical applications, Sci. Technol. Adv. Mat. 16 (2) (2015), https://doi.org/10.1088/1468-6996/16/2/023501.

[34] S. Fatimah, R. Ragadhita, D.F. Al Husaeni, A.B. Dani Nandiyanto, How to calculate crystallite size from X-ray diffraction (XRD) using Scherrer method, ASEAN, J. Sci. Eng. 2 (1) (2024) 65–76. ⟨https://ejournal.kjpupi.id/index.php/ajse/article/view/283⟩.

[35] Q. Lan, C. Liu, F. Yang, S. Liu, J. Xu, D. Sun, Synthesis of bilayer oleic acid-coated Fe_3O_4 nanoparticles and their application in pH-responsive Pickering emulsions, J. Colloid Interface Sci. 310 (1) (2007) 260–269, https://doi.org/10.1016/j.jcis.2007.01.081.

[36] H.Y. Hah, S. Gray, C.E. Johnson, J.A. Johnson, V. Kolesnichenko, P. Kucheryavy, G. Goloverda, Mössbauer spectroscopy of superparamagnetic Fe_3O_4 nanoparticles, J. Magn. Magn. Mater. 539 (2021) 168382, https://doi.org/10.1016/j.jmmm.2021.168382.

[37] D.S. Todorovsky, D.G. Dumanova, R.V. Todorovska, M.M. Getsova, Preparation and characterization of yttrium-iron citric acid complexes, Croat. Chem. Acta 75 (1) (2002) 155–164.

[38] N. Shukla, C. Liu, P.M. Jones, D. Weller, FTIR study of surfactant bonding to FePt nanoparticles, J. Magn. Magn. Mater. (2023) 178–184, https://doi.org/10.1016/S0304-8853(03)00469-4.

[39] J. Zou, Y.G. Peng, Y.Y. Tang, A facile bi-phase synthesis of Fe_3O_4@SiO_2 core-shell nanoparticles with tunable film thicknesses, RSC Adv. 4 (19) (2014) 9693–9700, https://doi.org/10.1039/c3ra47043a.

[40] J. Mohapatra, et al., Size-dependent magnetic and inductive heating properties of Fe_3O_4 nanoparticles: scaling laws across the superparamagnetic size, Phys. Chem. Chem. Phys. 20 (2018) 12879–12887, https://doi.org/10.1039/C7CP08631H.

[41] R.A. Harris, P.M. Shumbula, H. van der Walt, Analysis of the interaction of surfactants oleic acid and oleylamine with iron oxide nanoparticles through molecular mechanics modeling, Langmuir 31 (13) (2015) 3934–3943, https://doi.org/10.1021/acs.langmuir.5b00671.

[42] C.E. Johnson, J.A. Johnson, H.Y. Hah, et al., Mössbauer studies of stoichiometry of Fe_3O_4: characterization of nanoparticles for biomedical applications, Hyperfine Inter. 237 (2016) 27, https://doi.org/10.1007/s10751-016-1277-6.

[43] H.Y. Hah, Magnetism of Magnetite nanoparticles as determined by Mössbauer Spectroscopy. Masterś Thesis., University of Tennessee, Knoxville, 2016. ⟨https://trace.tennessee.edu/utk_gradthes/3773⟩.

[44] M. Guadaño-Sánchez, F. Navarro-Villoslada, G. Delgado-Soria, J.F. Marco, M. SauraMuzquiz, L. Álvaro-Gómez, P. de la Presa, L. Pérez, J.L. Urraca, Fast and straightforward synthesis in molecular imprinting: core–shell polymerization of magnetic imprinted polymers by microwave induction, ACS Appl. Polym. 6 (2024) 3243–3252, https://doi.org/10.1021/acsapm.3c03068.

[45] J. Fock, M.F. Hansen, C. Frandsen, S. Mørup, On the interpretation of Mössbauer spectra of magnetic nanoparticles, J. Magn. Magn. Mater. 445 (2018) 11–21, https://doi.org/10.1016/j.jmmm.2017.08.070.

[46] F.J. Berry, S. Skinner, M.F. Thomas, ^{57}Fe Mössbauer spectroscopic examination of a single crystal of Fe_3O_4, J. Phys. Condens. 10 (1998) 215, https://doi.org/10.1088/09538984/10/1/024.

[47] J. de la Figuera, J.F. Marco, Magnetite and the Verwey transition, from γ-rays to lowenergy electrons, Hyperfine Inter. 240 (2019) 44, https://doi.org/10.1007/s107510191577-8.

[48] R. Řezníček, V. Chlan, H. Štěpánková, P. Novák, J. Żukrowski, A. Kozłowski, Z. Kąkol, Z. Tarnawski, J.M. Honig, Understanding the Mössbauer spectrum of magnetite below the Verwey transition: Ab initio calculations, simulation, and experiment, Phys. Rev. B 96 (2017) 195124, https://doi.org/10.1103/PhysRevB.96.195124.

[49] R. Vandenberghe, C. Barrero, G. da Costa, et al., Mössbauer characterization of iron oxides and (oxy)hydroxides: the present state of the art, Hyperfine Interact. 126 (2000) 247–259, https://doi.org/10.1023/A:1012603603203.

[50] D.H. Han, J.P. Wang, H.L. Luo, Crystallite size effect on saturation magnetization of fine ferrimagnetic particles, J. Magn. Magn. Mater. 136 (1-2) (1994) 176–182, https://doi.org/10.1016/0304-8853(94)90462-6.

[51] M.H.R. Farimani, N. Shahtahmasebi, M. Rezaee Roknabadi, N. Ghows, A. Kazemi, Study of structural and magnetic properties of superparamagnetic Fe_3O_4/SiO_2 core-shell nanocomposites synthesized with hydrophilic citrate-modified Fe_3O_4 seeds via a sol-gel approach, Phys. E. Low. Dimens Syst. Nanostruct. 53 (2013) 207–216, https://doi.org/10.1016/j.physe.2013.04.032.

[52] E. Navarro-Palomares, et al., Dye-doped biodegradable nanoparticle SiO_2 coating on zinc- and iron-oxide nanoparticles to improve biocompatibility and for: In vivo imaging studies, Nanoscale 12 (10) (2020) 6164–6175, https://doi.org/10.1039/c9nr08743e.

[53] R. Rakhshaee, Y. Noorani, Comparing three methods of simultaneous synthesis and stabilization of Fe_3O_4 nanoparticles: changing physicochemical properties of products to improve kinetic and thermodynamic of dye adsorption, J. Magn. Magn. Mater. 422 (2017) 128–140, https://doi.org/10.1016/j.jmmm.2016.08.078.

[54] Z. Ge, T. Sun, J. Xing, X. Fan, Efficient removal of ethidium bromide from aqueous solution by using DNA-loaded Fe_3O_4 nanoparticles, Environ. Sci. Pollut. Res. *26* (2019) 2387–2396, https://doi.org/10.1007/s11356-018-3747-7.

[55] M.A. Dheyab, A.A. Aziz, M.S. Jameel, O.A. Noqta, P.M. Khaniabadi, B. Mehrdel, Simple rapid stabilization method through citric acid modification for magnetite nanoparticles, Sci. Rep. *10* (1) (2020) 10793, https://doi.org/10.1038/s41598-02067869-8.

[56] M. Qi, et al., Superparamagnetic Fe_3O_4 nanoparticles: Synthesis by a solvothermal process and functionalization for a magnetic targeted curcumin delivery system, N. J. Chem. 40 (5) (2016) 4480–4491, https://doi.org/10.1039/c5nj02441b.
[57] X. Liu, Y. Lu, Highly efficient and flexible preparation of water-dispersed Fe_3O_4 nanoclusters using a micromixer, Particuology 45 (2019) 42–48, https://doi.org/10.1016/j.partic.2018.06.003.
[58] R.O. da Silva, T.G. Conti, A.F. de Moura, D.G. Stroppa, L.C. Freitas, C. Ribeiro, et al., Antimony-doped tin oxide nanocrystals: synthesis and solubility behaviour in organic solvents, Chem. Phys. Chem. 10 (5) (2009) 841–846, https://doi.org/10.1002/cphc.200800764.
[59] M. Mahdi Eshaghi, M. Pourmadadi, A. Rahdar, A.M. Díez-Pascual, Novel carboxymethyl cellulose-based hydrogel with core–shell Fe_3O_4@SiO_2 nanoparticles for quercetin delivery, Materials 15 (24) (2022), https://doi.org/10.3390/ma15248711.